

Separating the effects of earthside and far side solar events. A case study

Silja Pohjolainen^{a,*}, Nasrin Talebpour Sheshvan^b, Christian Monstein^c

^a*Tuorla Observatory, Department of Physics and Astronomy, University of Turku, 20014 Turun yliopisto, Finland*

^b*Department of Physics and Astronomy, University of Turku, 20014 Turun yliopisto, Finland*

^c*Istituto ricerche solari Aldo e Cele Daccò (IRSOL), Faculty of Informatics, Università della Svizzera italiana (USI), CH-6605 Locarno, Switzerland*

Abstract

On 8 November 2013 a halo-type coronal mass ejection (CME) was observed, together with flares and type II radio bursts, but the association between the flares, radio bursts, and the CME was not clear. Our aim is to identify the origin of the CME and its direction of propagation, and to exclude features that were not connected to it. On the Earth-facing side, a GOES C5.7 class flare occurred close to the estimated CME launch time, followed by an X1.1 class flare. The latter flare was associated with an EUV wave and metric type II bursts. On the far side of the Sun, a filament eruption, EUV dimmings, and ejected CME loops were observed by imaging instruments onboard the Solar TERrestrial RELations Observatory (STEREO) spacecraft that were viewing the backside of the Sun. The STEREO radio instruments observed an interplanetary (IP) type II radio burst at decameter-hectometric wavelengths, which was not observed by the radio instrument onboard the Wind spacecraft located at L1 near Earth. We show that the halo CME originated from the eruption on the far side of the Sun, and that the IP type II burst was created by a shock wave ahead of the halo CME. The radio burst remained unobserved from the earthside, even at heliocentric source heights larger than 9 solar radii. During the CME propagation, the X-class flare eruption caused a small plasmoid ejection earthward, the material of which was superposed on the earlier CME structures observed in projection. The estimated heights of the metric type II burst match well with the EUV wave launched by the X-class flare. As this radio emission did not continue to lower frequencies, we conclude that the shock wave did not propagate any further. Either the shock driver died out, as a blast wave, or the driver speed no longer exceeded the local Alfvén speed.

© 2023 COSPAR. Published by Elsevier Ltd All rights reserved.

Keywords: Solar eruptions ; Coronal mass ejections ; Solar radio bursts

1. Introduction

Solar flares and eruptions are sometimes associated with propagating shock waves and coronal mass ejections (CMEs). The flare intensities, durations, eruption energetics, and mass sizes vary, and they do not necessarily depend on each other (Kawabata et al., 2018; Kahler and Ling, 2022). Many events are observed in projection, which makes it difficult to estimate source heights (Kwon, Zhang, and Vourlidas, 2015; Balmaceda et al., 2018; Vourlidas et al., 2020). Also separating far side events from Earth view events can be difficult for halo CMEs, as we cannot conclude the propagation direction if we only see a symmetrical halo surrounding the solar disc.

Flare-accelerated particles create emissions that can be observed especially in hard X-rays and microwaves. Microwave emission is typically due to trapped electrons gyrating in the closed magnetic field (gyrosynchrotron emission), and hard X-rays are created when some of these electron populations collide with dense material (often at the footpoints of flare loops). Plasma emission, on the other hand, is created when a transient propagates through a medium and causes oscillations that turn into radio waves at the local plasma frequency. Reviews on the various aspects of solar radio emission associated with solar events have been published by, e.g., Bastian, Benz, and Gary (1998), Nindos et al. (2008), and Pick and Vilmer (2008).

Observations at plasma frequencies include type III bursts which are created by electron beams that follow open magnetic field lines out from the Sun and into the interplanetary

*Corresponding author: silpoh@utu.fi

(IP) space. Propagating shock waves can create type II radio bursts, but the shock origin cannot always be determined (Fulara and Kwon, 2021; Chernov and Fomichev, 2021). Flare (blast) waves, driven waves, and bow shocks are all possible in connection with solar eruptions (Warmuth, 2007). Shock drivers can be fast CMEs or plasmoids, or fast expansion at the CME flanks. For bow shocks, the transient speed must exceed the local Alfvén speed.

Radio emission at plasma frequency is useful in a sense that it can be used to determine source heights. As plasma frequency depends only on the local electron density, we can use coronal density models to obtain estimates of distance from the solar surface. The conversion of radio frequency to atmospheric height has been reviewed in, e.g., Pohjolainen et al. (2007).

The research questions addressed in the present analysis are: Can we distinguish which parts of a halo CME are caused by far side eruption and which parts belong to frontside eruption? Can we exclude one or the other, based on observed flares and shock waves? Can radio emission help in separating source origins? We present a case study of multiple emissions and features that originated from active regions located on the earthside and the far side of the Sun, with possible associations to a halo CME.

2. Data analysis

We have analysed solar eruptions that occurred on 8 November 2013. Eruptions were observed on the earthside and the far side of the Sun, see Table 1. A halo CME was observed during the investigated time period of 00:00–06:00 UT.

For the analysis we used solar EUV images provided by the Atmospheric Imaging Assembly (AIA) (Lemen et al., 2012) onboard the Solar Dynamics Observatory (SDO), and the Extreme Ultraviolet Imager (EUVI) onboard the STEREO A and B spacecrafts (Wuelser et al., 2004). Coronagraph images and associated data products were obtained from the CDAW LASCO CME Catalog at <https://cdaw.gsfc.nasa.gov> that includes SOHO LASCO and STEREO A and B coronagraph images. Full-disc soft X-ray flux were provided by GOES satellites.

Radio data at decimeter-metric wavelengths include dynamic spectra from several e-CALLISTO Network stations (Benz, Monstein, and Meyer, 2005), <https://www.e-callisto.org/>, and from the Radio Solar Telescope Network (RSTN) Learmonth station, <https://www.ngdc.noaa.gov/stp/space-weather/solar-data/solar-features/solar-radio/rstn-spectral>. For interplanetary radio emission at decimeter-hectometric waves we used dynamic spectra from WAVES onboard the Wind satellite (Bougeret et al., 1995), and SWAVES spectra from the STEREO A and B satellites (Bougeret et al., 2008). These can be accessed in the CDAW LASCO CME Catalog. Microwave single frequency data were obtained from the Nobeyama radio polarimeters (NoRP) at <http://solar.nro.nao.ac.jp/norp/>.

Table 1. Flare/eruption times, locations, and intensities on 8 November 2013 for the time period of 00:00–06:00 UT. Two flares were listed to occur on the visible solar disc and a filament eruption was observed on the far side of the Sun. End times have been estimated from the GOES flux curves (not as in the NOAA flare listings). Only one CME was listed for this time period.

| Start time | End time | Location | GOES class/ or type |
|------------|----------|----------|-----------------------------|
| 02:25 UT | | S20W180 | Filament eruption southward |
| 02:33 UT | 03:10 UT | S18W25 | C5.7 |
| 04:20 UT | 04:45 UT | S14E15 | X1.1 |

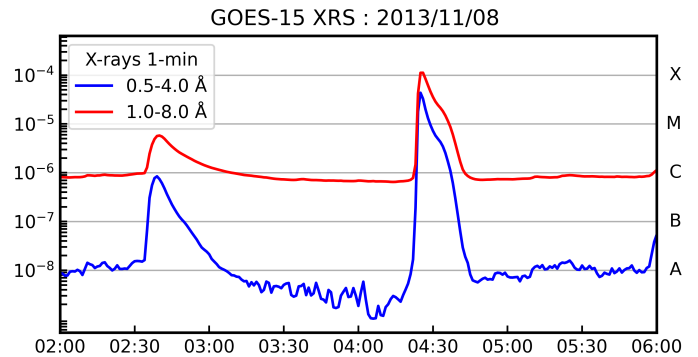


Fig. 1. GOES soft X-ray flux curve shows the C5.7 and X1.1 class flares.

2.1. Flares and eruptions

The first flare observed by GOES on 8 November 2013 is GOES class C5.7, start time at 02:33 UT, and duration of approximately 37 minutes, see Fig. 1. The flare is reported to have occurred at location S18W25 in NOAA active region (AR) 11891, and a corresponding small-scale loop brightening can be observed in the SDO/AIA images.

It is followed by a GOES X1.1 class flare in another region, in AR 11890 at location S14E15. The flare is reported to have a start time at 04:20 UT, flux peak time at 04:26 UT, and we estimated that the flare duration was approximately 25 minutes (Fig. 1).

This X-class flare was well-observed at microwaves and mm-waves, the peak flux reaching 4000 sfu at 17–35 GHz, and 2200 sfu at 80 GHz (Fig. 2). The flux began to rise at 04:23:40 UT, and multiple flux peaks were visible until 04:25:12 UT. Unfortunately no hard X-ray observations are available for this flare, but the high flux density at 80 GHz indicates particle acceleration to high energies.

Starting at 04:24 UT, decimeter-metric radio emission was observed by several ground-based stations. These emission structures are described in more detail in Section 2.2

The X-class flare was associated with a bubble-like EUV wave. The direction of the wave was southward from the AR, see Fig. 3. We measured the wave distances (dashed lines shown in Fig. 3) from the AR center at S14E15, assuming that the distance on the disc compares to the wave height. The distance increased from 0.333 R_{\odot} at 04:26 UT to 0.489 R_{\odot} at 04:28 UT, indicating a speed of approximately 900 km s^{-1} . In Fig. 2

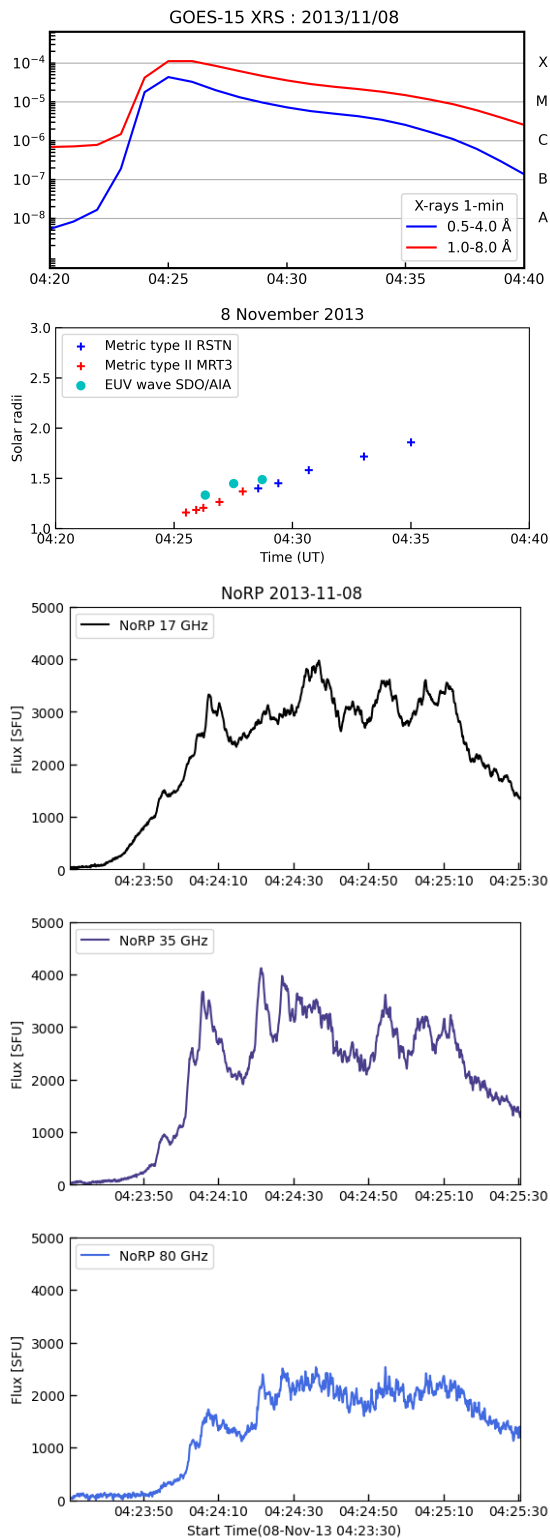


Fig. 2. Top: GOES X-rays from the X1.1 class flare. Middle: Estimated heliocentric distances/heights for the EUV wave (circles), and the metric type II burst (crosses) observed by e-CALLISTO MRT3 at 450–50 MHz and RSTN Learmonth at 180–25 MHz. The calculated radio source heights are listed in Table 2. Bottom three plots: Radio flux densities from the Nobeyama polarimeters at 17, 35, and 80 GHz, in the flare impulsive phase.



Fig. 3. SDO/AIA 193 Å difference images that show the evolution of the EUV wave that followed the GOES X1.1 class flare located at S14E15.

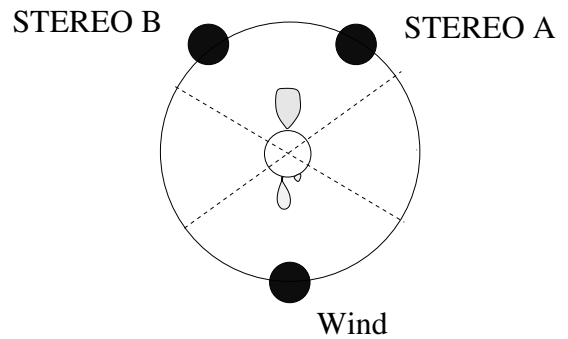
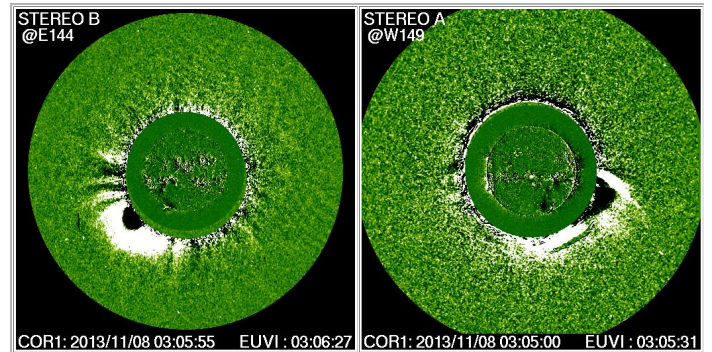


Fig. 4. Dimming regions and the launch of a CME on the far side of the Sun (STEREO A and B observations). The X-class flare on the earthside originated from an active region at E15, the C-class flare was a brightening at W25, and the far side eruption originated from a region near W180. Cartoon shows the locations of these eruptions, together with STEREO A and B positions. SOHO/LASCO and SDO have the same observing direction as Wind. The earthside flaring active regions at low heights were unobservable from STEREO A and B EUV imagers.

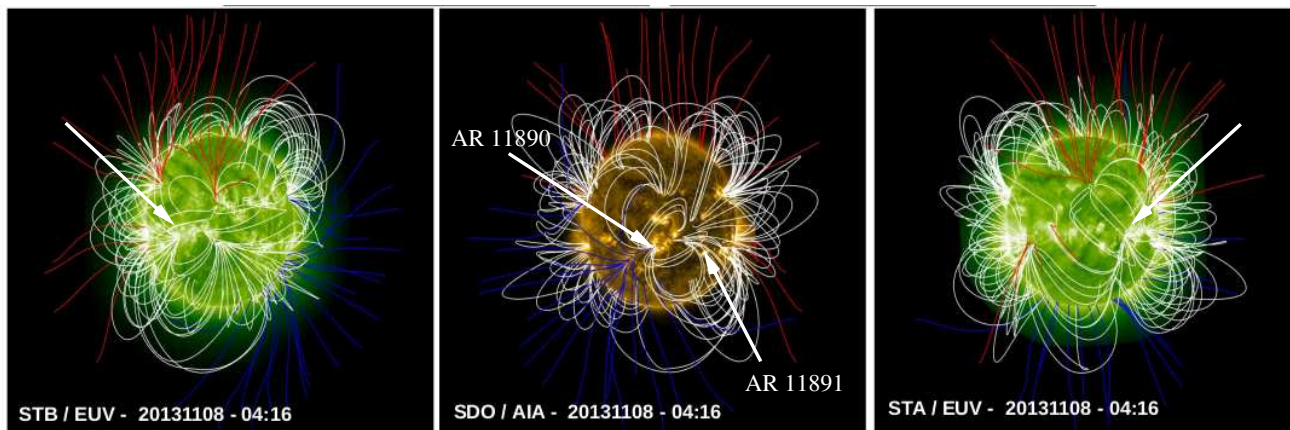


Fig. 5. Magnetic field lines calculated with the potential field source surface (pfss) model, shown in STEREO B, SDO, and STEREO A view. Active regions 11890 and 11891 are marked in the SDO view map, and white arrows mark the erupting region on the far side, near S20W180, in STEREO A and B views. Closed field lines are shown in white and open field lines in red and blue (opposite polarities).

the distances are shown in heliocentric heights, for comparison purposes.

On the far side of the Sun a filament eruption was observed at 02:25 UT. The most visible part of the filament was already at some distance from the AR location at S20W180, and it was directed toward south. STEREO A and B EUVI images show several dimming regions in the same direction (Fig. 4). Later on, dimmings appeared also in the location of the AR loops.

Potential field source surface (pfss) magnetic field lines were calculated using synoptic maps, as on the far side we have no direct magnetic field measurements. The field lines are shown both for Earth view and far side views in Fig. 5. They show that open field lines exist on the south-east side of AR 11890, but all other eruption regions lack open field lines in their vicinity. Flare-accelerated electrons would need open field lines to stream out from the Sun. Lack of type III bursts, especially in the interplanetary space, would also suggest that particles did not have access to any. For connectivity to observing particle detectors, it is useful to know where the open field lines are directed.

We note that the flaring regions AR 11890 and AR 11891 on the disc could not have been observed from STEREO A and B spacecraft, as they were located behind the limb in their field of views, see cartoon in Fig. 4.

2.2. Radio emission

Decimeter-metric radio emission started as narrow-width type III burst emission at ≈ 600 MHz at 04:24 UT. At 04:25 UT a clear type II burst emission lane became visible at 160 MHz, and it could be followed down to 30 MHz (e-CALLISTO and RSTN Learmonth dynamic spectra), see Fig. 7. The burst showed fundamental and harmonic emission lanes that were also band-split. The real start time of the burst is unclear, due to the overlap with other emission structures.

The metric type II burst did not continue to IP space (note that there is a data gap between 25 and 15 MHz, and therefore the end time and frequency cannot be determined). The disappearance of the type II burst may indicate that the shock wave

did not propagate any further. For example, a blast wave shock would eventually lose its energy and stop. For a bow shock a rise in the local Alfvén speed would make the shock die out if the transient speed no longer exceeded the local magnetosonic speed (note that the transient could still continue to move out at the same speed). To identify shock origin or shock driver is difficult without knowing the local plasma conditions, and without radio imaging at these wavelengths.

We estimated the metric type II burst heights from the e-CALLISTO MRT3 (Mauritius Radio Telescope, antenna number 3) and RSTN Learmonth dynamic spectra using the 'hybrid' coronal density model of Vršnak, Magdalenič, and Zlobec (2004). The derived instantaneous type II shock speeds were in the range of 670–980 km s⁻¹. As we do not know the local coronal densities but rely on the density model, this can be taken as an approximation of the shock speed. However, the radio emission heights and speeds are not far away from those of the EUV wave observed during the X-class flare. The metric type II burst heights are shown in Fig. 2 (cross symbols in the bottom plot), with the EUV wave distance/heights (circles). Type II burst frequencies and corresponding heights are listed in Table 2.

2.3. Coronal mass ejections and particles

On the far side of the Sun both STEREO COR1 coronagraphs observed a loop-shaped mass ejection at 03:05 UT (Fig. 4). The eruption that started at 02:25 UT, near location S20W180, and the following EUV dimmings match well with the CME shape and direction of propagation.

On the earthside a CME was first observed by SOHO LASCO at 03:24 UT, at height 2.7 R_⊙. The CME loop became fully visible in the next available LASCO C2 image at 03:47 UT. The CME speed, determined from LASCO observations, increased from 350 km s⁻¹ to 700 km s⁻¹ during the first seven hours of propagation (CDAW Catalog, 2nd order fit to the CME leading front heights).

A separate plasmoid structure was observed inside the CME loop at 05:12 UT, and its front was fully visible in the differ-

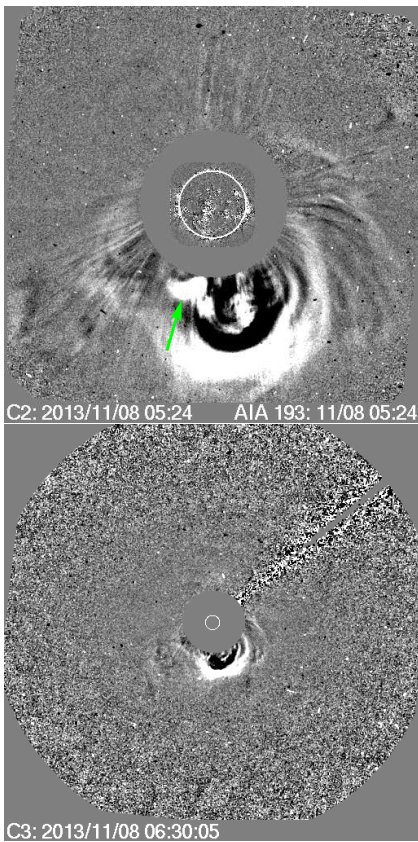
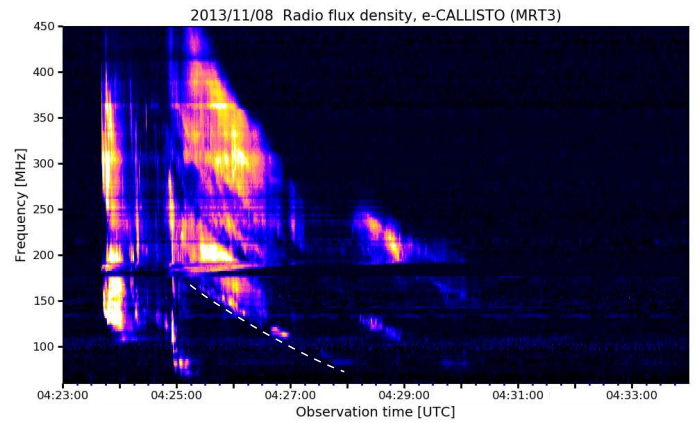
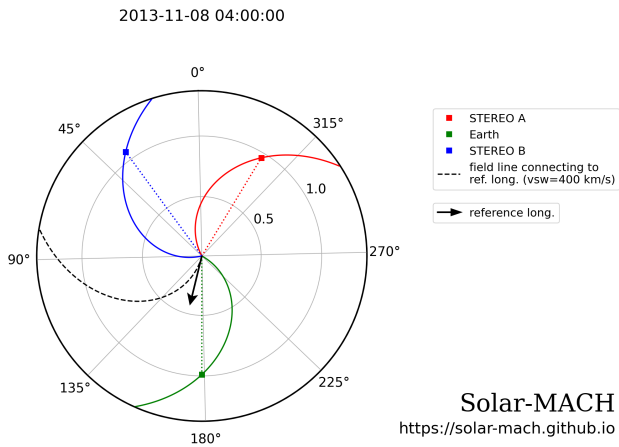


Fig. 6. Solar-MACH plot (prepared with the Solar MAGnetic Connection HAUS tool) shows the field line connecting to the reference longitude of the X1.1 class flare located at S14E15 (indicated with the dashed line, top). SOHO/LASCO C2 observation of the CME at 05:24 UT (middle). A separate plasmoid is visible, indicated with the green arrow. SOHO/LASCO C3 observation of the CME at 06:30 UT (bottom). During 06:00–07:00 UT an IP type II burst was observed by STEREO A and B, but not by Wind.

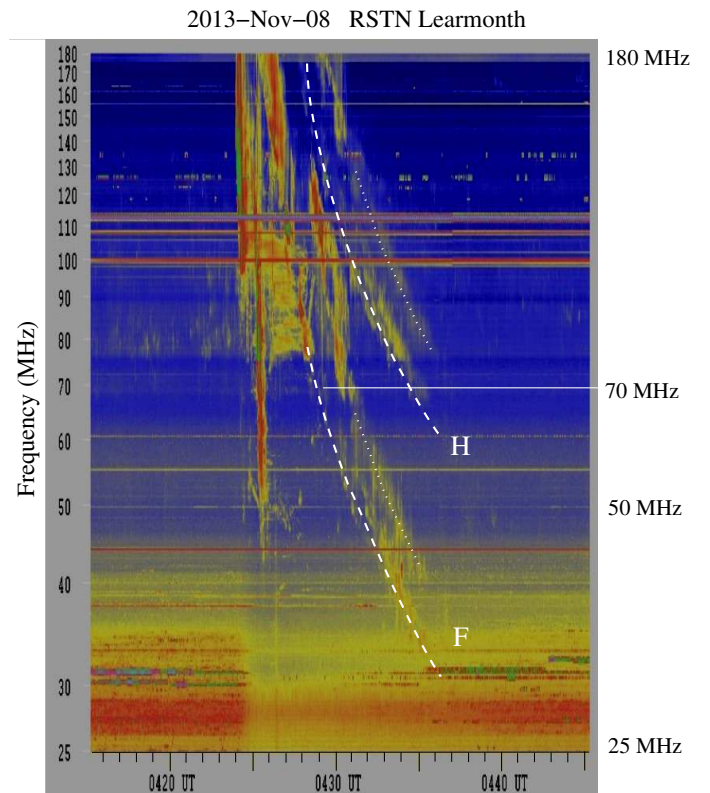


Fig. 7. Tracing the type II lanes in the e-CALLISTO MRT3 dynamic spectrum in the frequency range of 450–50 MHz (top) and in the RSTN Learmonth spectrum at 180–25 MHz (bottom). The fundamental (F) and harmonic (H) lanes are band-split (indicated with dashed and dotted lines in the Learmonth spectrum, respectively). We used the fundamental, lower band-split lane in the height calculations. The times and heights are listed in Table 2 and they are shown in Figs. 2 and 9. The type II emission was preceded by type III bursts, which makes it difficult to define the exact type II burst start time.

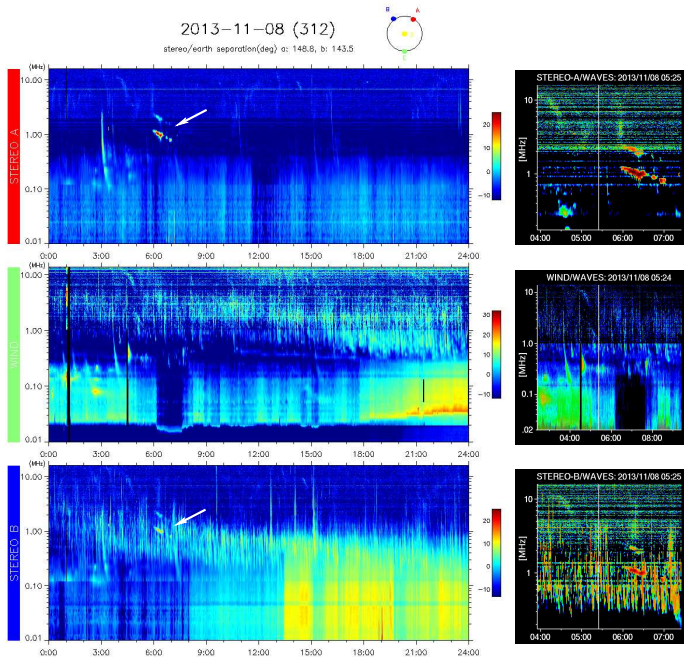


Fig. 8. STEREO A/SWAVES (location A in red), Wind/WAVES (location in green), and STEREO B/SWAVES (location B in blue) dynamic radio spectra from ≈ 10 MHz down to 10 kHz. The visible IP type II burst lanes are indicated with arrows.

ence image at 05:24 UT, see Fig. 6 (the front is indicated with a green arrow). The speed of this structure was estimated to be 400 km s^{-1} . After 05:48 UT it could not be distinguished from the bright main loop any longer.

The CME and plasmoid heights are shown in Fig. 9, where they are presented together with the radio source heights that are discussed in Section 2.2.

We checked in-situ particle measurements from both STEREO spacecraft and Wind. A high-speed halo CME that was launched the day before, near 10 UT on 7 November and originating also from the far side, caused an increase in proton and electron intensities in STEREO A and B particle detectors. The intensities remained high also on 8 November, making it difficult to separate later enhancements. The 7 November flare-CME-SEP event is described in detail in Dresing et al. (2016).

In the interplanetary space, below 15 MHz frequencies, very few type III bursts are observed. Dynamic spectrum from STEREO A shows a type III burst at 03:04 UT, first appearing at 2.5 MHz (height $\approx 6 R_{\odot}$), and Wind/WAVES shows a very faint type III burst appearing at 03:45 UT at 4 MHz. This indicates that despite the flaring activity and CME propagation, few accelerated particles had access to open field lines. The Solar-MACH plot in Fig. 6 shows how the field line from the X-class flare location is not connected to any of the spacecraft, see Gieseler et al. (2023) on how the visualization of the spatial configuration and the solar magnetic connection to different observers is done.

An IP type II burst was observed by STEREO A and B, appearing at 1.2 MHz frequency at 06:00 UT. This type II burst

Table 2. Estimated type II burst heights. We used meter-wave observations from e-CALLISTO MRT3 and RSTN Learmonth, and DH-wave observations are from STEREO A and B SWAVES. Heights are heliocentric and they are calculated from emission at the fundamental plasma frequency, see text for details.

| Time | Frequency | Height |
|-------------|-----------|-------------------|
| 04:25:30 UT | 163 MHz | $1.16 R_{\odot}$ |
| 04:25:56 UT | 147 MHz | $1.18 R_{\odot}$ |
| 04:26:14 UT | 135 MHz | $1.21 R_{\odot}$ |
| 04:26:55 UT | 111 MHz | $1.26 R_{\odot}$ |
| 04:27:54 UT | 83 MHz | $1.37 R_{\odot}$ |
| 04:28:33 UT | 78.1 MHz | $1.40 R_{\odot}$ |
| 04:29:24 UT | 70.0 MHz | $1.45 R_{\odot}$ |
| 04:30:41 UT | 54.9 MHz | $1.58 R_{\odot}$ |
| 04:33:01 UT | 44.2 MHz | $1.72 R_{\odot}$ |
| 04:35:00 UT | 36.2 MHz | $1.86 R_{\odot}$ |
| 06:00 UT | 1.22 MHz | $9.20 R_{\odot}$ |
| 06:10 UT | 1.12 MHz | $9.65 R_{\odot}$ |
| 06:20 UT | 1.00 MHz | $10.36 R_{\odot}$ |
| 06:30 UT | 1.02 MHz | $10.16 R_{\odot}$ |
| 06:45 UT | 930 kHz | $10.71 R_{\odot}$ |
| 06:55 UT | 815 kHz | $11.56 R_{\odot}$ |
| 07:02 UT | 790 kHz | $11.77 R_{\odot}$ |

was not observed by Wind (located in L1 on the Earth-facing side), see Fig. 8. The type II burst emission lane could be followed down to 700 kHz, where the emission ended around 07:00 UT. The calculated source heights, using the fundamental emission lane and the same 'hybrid' density model, are listed in Table 2.

The radio source heights, with all other feature heights we have identified and analysed, are plotted in Fig. 9 for comparison. From this plot it is evident that the IP type II burst heights correspond to the CME leading front heights observed from the far side, and that the earthside LASCO observations of the CME fronts have lower heights. Far side CME heights in Fig. 9 are from STEREO B, as STEREO A observations show a wider CME structure, almost a double loop, with several fronts. However, the heights of the leading parts are similar to the STEREO B observations. LASCO height measurements most probably suffer from projection effects, as the halo CME originated from almost exactly the opposite side of the Sun. This may well explain the lower heights.

The height-time evolution indicates that the metric type II burst and the IP type II burst are not connected, but were created by separate propagating shock waves.

3. Summary and conclusions

We have analysed features and emissions that could have been associated with a halo CME on 8 November 2013. We wanted to identify the origin of the CME, and to exclude features that were not connected to it. As eruptions were observed both on the earthside and on the far side of the Sun, detailed analysis was needed. In halo CMEs the bright coronal emission is observed in projection around the solar disk, and from coro-

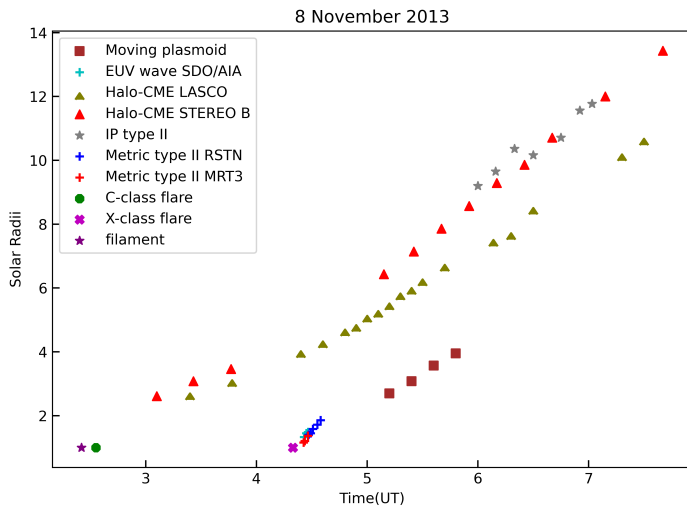


Fig. 9. Measured and calculated heights of all propagating structures. For flares and filament eruption we show their start times.

nagraph images only it is impossible to conclude if the CME is launched toward Earth or in the opposite direction.

After investigating the eruptions and flares, some followed by EUV waves and dimmings, and estimating the type II radio burst heights, we conclude that the halo CME originated from the eruption on the far side of the Sun. The IP type II burst was created by a shock wave (bow shock) ahead of the halo CME, but the radio burst location was invisible to Earth. The most probable reason for not observing it would be dense plasma structures blocking wave propagation. An example of this kind of configuration is presented in Fig. 11 in Talebpour Sheshvan and Pohjolainen (2018). If the radio source was located in a region directed towards STEREO A and B, also the solar disc, or the CME itself, could have blocked radio emission toward the Earth.

It is well known that type II bursts are typically formed in narrow regions somewhere along the shock front, where plasma conditions are favourable. The relatively short duration and narrow band of the IP type II burst, and late appearance after the CME launch, suggest that the radio emission could have been caused by interaction with a small-volume ambient plasma structure.

During the CME propagation, the X-class flare eruption on the earthside of the Sun caused a small plasmoid ejection, the material of which was superposed on the halo CME features. The estimated heights of the metric type II burst match well with the EUV wave launched by the X-class flare, and the height-time trajectory of the plasmoid suggests they could be associated. As the type II burst emission did not continue to IP space, we conclude that either the shock died out (as a blast wave), or an increase in the local Alfvén speed made it impossible to propagate further out.

4. Acknowledgments

We thank the e-CALLISTO community for free access to their data and software. MRT3 is located and operated at Uni-

versity of Mauritius, Poste de Flacq, Mauritius. The Radio Solar Telescope Network (RSTN) is a network of solar observatories maintained and operated by the US Air Force. Learmonth is located in Australia and their data is included in Space Weather databases. Nobeyama Radio Polarimeters (NoRP) are operated by Solar Science Observatory, a branch of National Astronomical Observatory of Japan. The CME Catalog is generated and maintained at the CDAW Data Center by NASA and the Catholic University of America in cooperation with the Naval Research Laboratory.

References

- Balmaceda, L.A., Vourlidas, A., Stenborg, G., Dal Lago, A., 2018. How Reliable Are the Properties of Coronal Mass Ejections Measured from a Single Viewpoint? *Astrophys. J.* 863, id. 57. <https://doi.org/10.3847/1538-4357/aacff8/>
- Bastian, T.S., Benz, A.O., Gary, D.E., 1998. Radio Emission from Solar Flares. *Ann. Rev. Astron. Astrophys.* 36, 131-188. <https://doi.org/10.1146/annurev.astro.36.1.131>
- Benz, A.O., Monstein, C., Meyer, H., 2005. Callisto A New Concept for Solar Radio Spectrometers. *Solar Phys.* 226, 143-151. <https://doi.org/10.1007/s11207-005-5688-9/>
- Bougeret, J.-L., Goetz, K., Kaiser, M.L., Bale, S.D., Kellogg, P.J., Maksimovic, M., et al., 2008. S/WAVES: The Radio and Plasma Wave Investigation on the STEREO Mission. *Space Sci. Rev.* 136, 487-528. <https://doi.org/10.1007/s11214-007-9298-8>
- Bougeret, J.-L., Kaiser, M.L., Kellogg, P.J., Manning, R., Goetz, K., Monson, S.J., Monge, N., Friel, L., Meete, C. A., Perche, C., Sitruk, L., Hoang, S., 1995. WAVES: The radio and plasma wave investigation on the wind spacecraft. *Space Sci. Rev.* 71, 231-263. <https://doi.org/10.1007/BF00751331>
- Chernov, G., Fomichev, V., 2021. On the Issue of the Origin of Type II Solar Radio Bursts. *Astrophys. J.* 922, id.82. <https://doi.org/10.3847/1538-4357/ac1f32>
- Dresing, N., Gómez-Herrero, R., Heber, B., Hidalgo, M.A., Klassen, A., Temmer, M., Veronig, A., 2016. Injection of solar energetic particles into both loop legs of a magnetic cloud. *Astron. Astrophys.* 586, id. A55. <https://doi.org/10.1051/0004-6361/201527347>
- Gieseler, J., Dresing, N., Palmroos, C., Freiherr von Forstner, J.L., Price, D.J., Vainio, R., et al., 2022. Solar-MACH: An open-source tool to analyze solar magnetic connection configurations. *Front. Astronomy Space Sci.* 9, id. 384. <https://doi.org/10.3389/fspas.2022.1058810>
- Fulara, A., Kwon, R.-Y., 2021. Global Nature of Solar Coronal Shock Waves Shown by Inconsistency between EUV Waves and Type II Radio Bursts. *Astrophys. J. Lett.* 919, id.L7. <https://doi.org/10.3847/2041-8213/ac230d>
- Kahler, S.W., Ling, A.G., 2022. A Comparison of Solar X-Ray Flare Timescales and Peak Temperatures with Associated Coronal Mass Ejections. *Astrophys. J.* 934, id.175. <https://doi.org/10.3847/1538-4357/ac7e56>
- Kawabata, Y., Iida, Y., Doi, T., Akiyama, S., Yashiro, S., Shimizu, T., 2018. Statistical Relation between Solar Flares and Coronal Mass Ejections with Respect to Sigmoidal Structures in Active Regions. *Astrophys. J.* 869, id. 99. <https://doi.org/10.3847/1538-4357/aebfc>
- Kwon, R.-Y., Zhang, J., Vourlidas, A., 2015. Are Halo-like Solar Coronal Mass Ejections Merely a Matter of Geometric Projection Effects? *Astrophys. J. Lett.* 799, id. L29. <https://doi.org/10.1088/2041-8205/799/2/L29>
- Lemen, J.R., Title, A.M., Akin, D.J., Boerner, P.F., Chou, C., Drake, J.F., Duncan, D.W., Edwards, C.G., Friedlaender, F.M., Heyman, G. F., et al., 2012. The Atmospheric Imaging Assembly (AIA) on the Solar Dynamics Observatory (SDO). *Solar Phys.* 275, 17-40. <https://doi.org/10.1007/s11207-011-9776-8>
- Nindos, A., Aurass, H., Klein, K.-L., Trottet, G., 2008. Radio Emission of Flares and Coronal Mass Ejections. *Invited Review. Solar Phys.* 253, 3-41. <https://doi.org/10.1007/s11207-008-9258-9>
- Pick, M., Vilmer, N., 2008. Sixty-five years of solar radioastronomy: flares, coronal mass ejections and Sun Earth connection. *Astron. Astrophys. Rev.* 16, 1-153. <https://doi.org/10.1007/s00159-008-0013-x>
- Pohjolainen, S., van Driel-Gesztelyi, L., Culhane, et al., 2007. CME Propa-

- gation Characteristics from Radio Observations. *Solar Phys.* 244, 167-188. <https://doi.org/10.1007/s11207-007-9006-6>
- Talebpour Sheshvan, N., Pohjolainen, S., 2018. Visibility and Origin of Compact Interplanetary Radio Type IV Bursts. *Solar Phys.* 293, id. 148. <http://doi.org/10.1007/s11207-018-1371-9>
- Vourlidas, A., Balmaceda, L.A., Xie, H., St. Cyr, O.C., 2020. The Coronal Mass Ejection Visibility Function of Modern Coronagraphs. *Astrophys. J.* 900, id. 161. <http://doi.org/10.3847/1538-4357/abada5>
- Vršnak, B., Magdalenic, J., Zlobec, P., 2004. Band-splitting of coronal and interplanetary type II bursts. III. Physical conditions in the upper corona and interplanetary space. *Astron. Astrophys.* 413, 753-763. <http://doi.org/10.1051/0004-6361:20034060>
- Warmuth, A., 2007. Large-scale Waves and Shocks in the Solar Corona. In KL. Klein and A.L. MacKinnon (eds.), *The High Energy Solar Corona: Waves, Eruptions, Particles.* *Lect. Notes Phys.* 725, 107-138. https://doi.org/10.1007/978-3-540-71570-2_6
- Wueller, J.-P., Lemen, J.R., Tarbell, T.D., Wolfson, C.J., Cannon, J.C., Carpenter, B.A., Duncan, D.W., Gradwohl, G.S., Meyer, S.B., Moore, A.S., et al., 2004. EUVI: the STEREO-SECCHI extreme ultraviolet imager, in S. Fineschi and M.A. Gummin (eds.), *Telescopes and Instrumentation for Solar Astrophysics.* *Proc. SPIE* 5171, 111-122. <https://doi.org/10.1117/12.506877>